

# DepthVision: Robust Vision-Language Understanding through GAN-Based LiDAR-to-RGB Synthesis

Sven Kirchner<sup>1</sup>, Nils Purschke<sup>1</sup>, Ross Greer<sup>2</sup> and Alois C. Knoll<sup>1</sup>

**Abstract**—Ensuring reliable robot operation when visual input is degraded or insufficient remains a central challenge in robotics. This letter introduces DepthVision, a framework for multimodal scene understanding designed to address this problem. Unlike existing Vision-Language Models (VLMs), which use only camera-based visual input alongside language, DepthVision synthesizes RGB images from sparse LiDAR point clouds using a conditional generative adversarial network (GAN) with an integrated refiner network. These synthetic views are then combined with real RGB data using a Luminance-Aware Modality Adaptation (LAMA), which blends the two types of data dynamically based on ambient lighting conditions. This approach compensates for sensor degradation, such as darkness or motion blur, without requiring any fine-tuning of downstream vision-language models. We evaluate DepthVision on real and simulated datasets across various models and tasks, with particular attention to safety-critical tasks. The results demonstrate that our approach improves performance in low-light conditions, achieving substantial gains over RGB-only baselines while preserving compatibility with frozen VLMs. This work highlights the potential of LiDAR-guided RGB synthesis for achieving robust robot operation in real-world environments.

## I. INTRODUCTION

Robot tasks often rely on the accurate perception of the environment, including static objects and the predicted motion of dynamic objects and agents [1], [2], [3], [4], [5], [6]. Such perception, prediction, and planning tasks have recently experienced significant advances through Vision-Language Models (VLM) and Vision-Language-Action models (VLA), including the introduction of end-to-end pipelines that map sensor input directly to control signals. Embodied multimodal language models (EMLMs) extend large pretrained language models (LLMs) with continuous sensor streams from robotic platforms, thereby enabling complex closed-loop control capabilities [7]. Transformer-based architectures, leveraging the Self-Attention and Multi-Head Attention mechanisms introduced in [8], have demonstrated the capacity to directly map raw vision inputs (e.g., camera images) and natural language instructions to robot actions [9]. Unified sequence models with object-centric, multimodal prompting further expand the range of tasks that can be solved within a single model architecture, supporting general-purpose manipulation and interaction [10]. These

developments critically depend on sufficiently rich visual information to perceive relevant objects and scene dynamics and to inform downstream decision-making processes. Despite these advances, the rapid development of VLA models raises fundamental questions about the trade-offs, costs and limitations of current multimodal sensing strategies. While camera images provide dense semantic information, additional sensing modalities—such as LiDAR—enhance spatial awareness and physical obstacle detection, especially in low-light or poor-visibility conditions where cameras may struggle, though this comes at the cost of increased hardware complexity and expense. Vision Transformers (ViTs) scale favorably with model and dataset size, given abundant training data [11]. However, the availability of web-scale multimodal datasets—spanning images and text—has predominantly benefited vision-based learning, as vast quantities of annotated visual data are readily available through online repositories, social media and public datasets [12].

In contrast, LiDAR data remain scarce at scale, given the inherent costs and logistical barriers to mass collection and labeling of point clouds. Unlike images or videos, which are easily generated and shared by consumers, LiDAR scans and dense depth point clouds are rarely produced or published in large, diverse quantities. As a result, current foundation models overwhelmingly favor the visual modality, limiting the robustness of models deployed in real-world tasks that require accurate three-dimensional spatial reasoning. This challenge is increasingly relevant in robotics domains such as autonomous driving, where robust and reliable multimodal sensor fusion remains an open research question [13]. Therefore, developing methods for processing multimodal sensors that balance the strengths and limitations of vision- and range-based data is a critical next step for the field.

Therefore, we propose DepthVision: a robust, multimodal framework that enables Vision-Language Models to maintain high performance, even when the real camera signal is degraded, unavailable or unreliable, by leveraging LiDAR sensing as an alternative modality. By synthesizing photorealistic RGB images from LiDAR data and adaptively fusing them with real camera input, DepthVision substantially improves scene understanding in challenging conditions such as low light, occlusion, or sensor failure.

The main contributions are:

- A GAN-based architecture with an integrated refiner that synthesizes RGB scene images directly from sparse LiDAR range data.
- Two luminance-aware fusion mechanisms that adaptively combine real and synthetic visual inputs for robust

This work was supported by the Federal Ministry of Research, Technology and Space (BMFTR) as part of the CeCaS project, FKZ: 16ME0800K.

<sup>1</sup>Sven Kirchner, Nils Purschke and Alois C. Knoll are with the Chair of Robotics, Artificial Intelligence and Real-time Systems, Technical University of Munich, 80333 Munich, Germany (email: sven.kirchner@tum.de)

<sup>2</sup>Ross Greer is with the Computer Science and Engineering Department, University of California Merced, Merced, CA 95343 USA

downstream processing.

- Comprehensive experiments showing the benefits of the generated representations, enhancing scene understanding for robot operation under adverse illumination conditions.

## II. RELATED WORK

*Vision–Language–Action Models in Robotics.* Recent advances in robotics highlight the growing role of Vision–Language–Action Models in bridging robotic perception, reasoning and control. These models are being applied across core robotic tasks: zero-shot trajectory generation [14], multimodal task planning [15], adaptive task replanning [16], navigation [17] and resource-efficient robotic manipulation [18]. Although targeting different robotic domains, all approaches depend critically on robust scene understanding. This has motivated research into multimodal sensor fusion and the enrichment of RGB images with depth data [19], with the aim of improving perception, even in challenging conditions. Collectively, these works demonstrate that reliable multimodal perception is fundamental to deploying VLM- and VLA-based systems in robotics, particularly for safety-critical operation in unstructured real-world environments.

*Vision–Language Models and multimodality.* Large-scale Vision–Language Models have demonstrated strong performance on tasks that require joint reasoning over images and text. These models extend pretrained language backbones by integrating visual encoders, enabling complex tasks such as multimodal dialogue, image captioning, visual question answering and instruction following. A foundational enabler of modern VLMs is the Vision Transformer (ViT)[20], which adapts the self-attention mechanism originally developed for natural language processing to the visual domain. Since a naive application of self-attention at the pixel level would be computationally prohibitive, ViTs restructure an image  $\mathbf{x} \in \mathbb{R}^{H \times W \times C}$  into a sequence of flattened 2D patches  $\mathbf{x}_p \in \mathbb{R}^{N \times (P^2 C)}$ , where  $(H, W)$  is the image resolution,  $C$  the number of channels,  $P \times P$  the patch size and  $N = HW/P^2$  the resulting sequence length. This allows the image to be processed in the same way as a token sequence in text, unlocking scalable multimodal attention. While conventional computer vision pipelines focus on predicting a fixed set of object classes, VLMs instead learn to align visual and linguistic modalities in a shared embedding space [21]. For example, models like VisualBERT [22] jointly process visual and textual inputs by embedding region-based visual features and text tokens, which are then fed into a single transformer encoder. The model is pretrained using masked language modeling and an image–text matching objective, enabling it to learn rich cross-modal representations. Some vision–language models, such as FLAVA [23], extend this idea by employing a fully shared transformer encoder across both modalities, supporting unified learning over image, text and multimodal inputs. Recent work has begun adapting VLMs to incorporate 3D data. Chen et al. [24] leverage monocular metric depth estimation to lift large-scale 2D internet images into metric 3D point clouds, enhancing the 3D

scene understanding and question answering capabilities of vision–language models. Yang et al. [25] propose integrating LiDAR data with large language models by flattening the 3D point cloud along the z-axis to generate a bird’s-eye-view (BEV) feature map, which is then used as a prompt input to a view-aware transformer module within the LLM.

*Generative Adversarial Networks and refiner.* Generative Adversarial Networks (GANs) were first introduced by Goodfellow et al.[26] as a framework for generating realistic synthetic data through an adversarial game between a generator and a discriminator. The Deep Convolutional GAN (DCGAN)[27] extended this idea by using deep convolutional layers to improve stability and visual quality in image generation tasks. For image-to-image translation, architectures such as the U-Net [28] are widely used because their encoder–decoder structure with skip connections helps preserve spatial details. The pix2pix framework [29] applied conditional GANs to learn mappings between paired image domains, making it suitable for tasks like translating depth maps into RGB images. To improve the quality of generated images, Shrivastava et al. [30] proposed adding a refiner network that cleans and enhances synthetic outputs, making them more realistic. This is especially important for ill-posed problems where the input data is sparse or incomplete. For example, generating a three-channel RGB image from a single-channel depth map requires the network to hallucinate missing color and texture information. One effective strategy for handling such under-constrained mappings is to use iterative refinement methods [31]. Instead of generating the final image in a single step, the network produces an initial estimate and then improves it in multiple stages using a learned or fixed update rule. This step-by-step approach helps the model converge to a higher-quality result with better structural consistency and fewer artifacts.

## III. METHOD

In this work, we present a multimodal scene understanding framework, outlined in Fig. 1. Given LiDAR point clouds, RGB images and textual input, we first project the 3D LiDAR data into the 2D image plane using calibrated sensor parameters (Section III-A). We then generate synthetic RGB images from the projected LiDAR data using a U-Net-based GAN (Section III-B). To ensure robustness under adverse conditions such as poor lighting or sensor occlusion, we estimate the mean luminance of the RGB input and adaptively adjust the contribution of each modality (Section III-C). Finally, we integrate all inputs into a unified vision–language transformer, which performs joint reasoning over fused LiDAR-image and text embeddings (Section III-D).

### A. LiDAR Preprocessing

To align LiDAR data with the RGB camera, we perform a standard 3D-to-2D projection using calibrated sensor parameters. Each LiDAR point  $\mathbf{X}_{\text{LiDAR}}^i = [x^i, y^i, z^i, 1]^T \in \mathbb{R}^4$  is transformed into the camera frame using the extrinsic

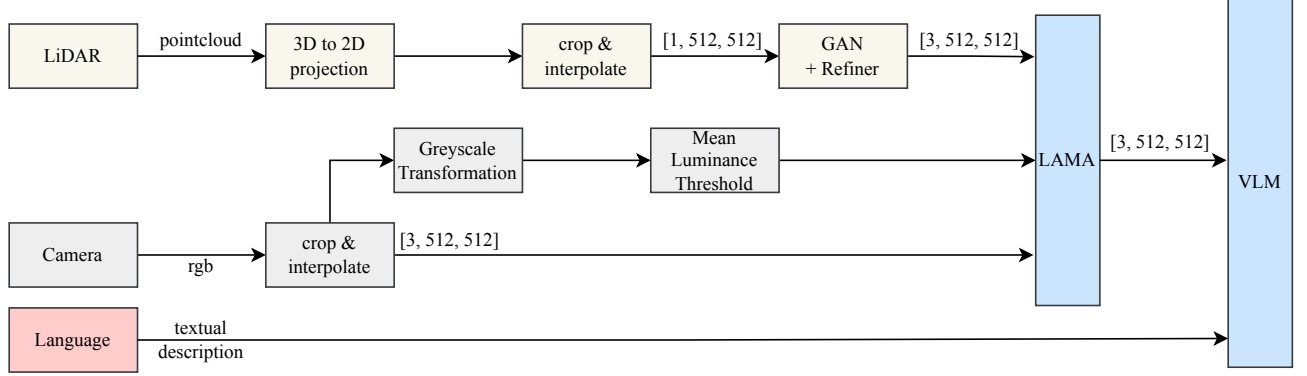


Fig. 1: The DepthVision architecture consists of four main components: the LiDAR processing pipeline; RGB image processing; the Luminance-Aware Modality Adaptation (LAMA) module; and the Vision–Language Model.

transformation:

$$\mathbf{X}_c^i = \mathbf{T}_{\text{cam} \leftarrow \text{LiDAR}} \cdot \mathbf{X}_{\text{LiDAR}}^i, \quad \mathbf{T}_{\text{cam} \leftarrow \text{LiDAR}} = \begin{bmatrix} \mathbf{R} & \mathbf{t} \\ \mathbf{0}^\top & 1 \end{bmatrix} \in \mathbb{R}^{4 \times 4} \quad (1)$$

where  $\mathbf{R} \in \mathbb{R}^{3 \times 3}$  is the rotation matrix and  $\mathbf{t} \in \mathbb{R}^3$  is the translation vector between the LiDAR and camera coordinate frames. The transformed points  $\mathbf{X}_c^i = (X_c^i, Y_c^i, Z_c^i)$  are then projected onto the image plane using the camera intrinsic matrix  $\mathbf{K} \in \mathbb{R}^{3 \times 3}$ :

$$\mathbf{x}_{\text{pix}}^i = \mathbf{K} \cdot \begin{bmatrix} X_c^i/Z_c^i \\ Y_c^i/Z_c^i \\ 1 \end{bmatrix}, \quad \mathbf{K} = \begin{bmatrix} f_x & 0 & c_x \\ 0 & f_y & c_y \\ 0 & 0 & 1 \end{bmatrix} \quad (2)$$

yielding pixel coordinates  $(u^i, v^i)$ :

$$u^i = f_x \cdot \frac{X_c^i}{Z_c^i} + c_x, \quad v^i = f_y \cdot \frac{Y_c^i}{Z_c^i} + c_y \quad (3)$$

where  $f_x, f_y$  are the focal lengths in pixels and  $c_x, c_y$  denote the coordinates of the camera’s principal point (optical center) in the image plane.

Only points that are both in front of the camera and within the image bounds are retained, i.e., those satisfying:

$$Z_c^i > 0, \quad 0 \leq u^i < W, \quad 0 \leq v^i < H \quad (4)$$

where  $W$  and  $H$  denote the image width and height in pixels, respectively. After this, the resulting image is cropped to  $600 \times 600$  pixels centered around the principal point. To construct a dense 2D representation from the sparsely projected points, we apply nearest-neighbor interpolation, which preserves sharp edges and discrete values without introducing smoothing artifacts. This is particularly important to compress the LiDAR data even more, while maintaining spatial sparsity and depth discontinuities is critical for downstream tasks. Given a projected 2D coordinate  $(u^i, v^i)$ , the nearest-neighbor interpolation selects the value from the closest available LiDAR point in the discrete image grid:

$$\hat{D}(u, v) = D \left( \arg \min_{(i,j) \in \Omega} \sqrt{(u-i)^2 + (v-j)^2} \right) \quad (5)$$

where  $D$  is the sparse depth map and  $\Omega$  is the set of pixels with valid LiDAR projections.

### B. GAN and Refiner Setup

To synthesize RGB images from projected LiDAR inputs, we use a conditional Generative Adversarial Network (GAN) (See Fig. 2) based on the widely used *pix2pix* framework [29], with RGB images normalized across all three channels to the range  $[-1, 1]$ . The generator uses a U-Net-style encoder–decoder architecture with skip connections between corresponding layers to preserve spatial detail. This design enables the model to learn structured mappings from sparse LiDAR projections to dense RGB domains, while retaining edge information.

The generator receives as input a single-channel LiDAR projection image of size  $512 \times 512$  and outputs a three-channel RGB image of identical resolution. This generated image serves as input to the subsequent VLM, ensuring robustness in multimodal tasks even when real RGB data is degraded or unavailable (e.g., due to poor lighting).

The discriminator is trained in a PatchGAN style, evaluating the realism of local  $70 \times 70$  patches in the image rather than the full image at once. This local-level supervision encourages high-frequency detail and texture fidelity.

To further improve the fidelity of the synthesis, we use a dedicated refiner module to perform residual refinement through iterative correction. The refiner is defined as a fully convolutional, compact network comprising three convolutional layers with ReLU activations and a final tanh to bound the residual output within  $[-1, 1]$ . At each iteration, the current RGB estimate and LiDAR projection are fused and passed through the refiner, which predicts a residual term subsequently added to the RGB input. This procedure is applied for three iterations to iteratively suppress high-frequency artifacts and enhance structural coherence.

The output of the generation process is first fused with the RGB image using weighted fusion. This ensures that the vision language model downstream benefits from a dense, RGB-like representation, even in scenarios where original camera data is missing or corrupted.

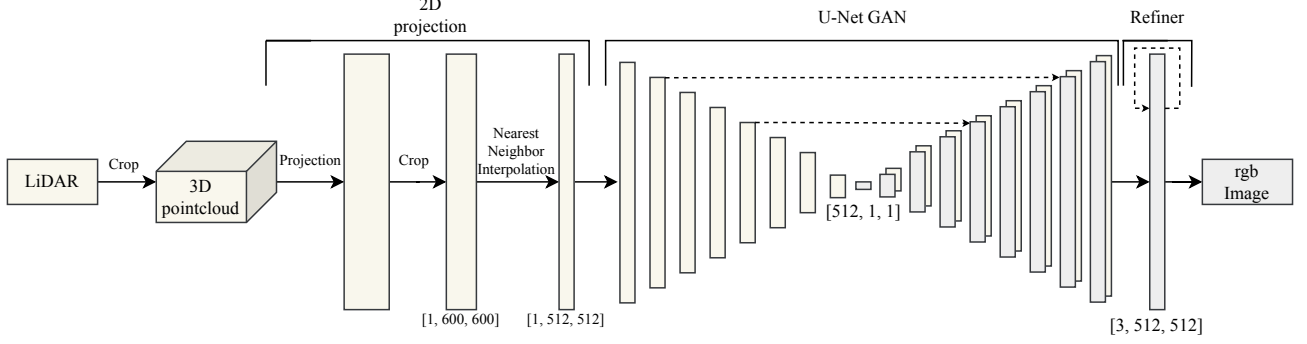


Fig. 2: The LiDAR processing pipeline.

### C. Luminance-Aware Modality Adaptation (LAMA)

To enable robust scene understanding under varying illumination conditions, we introduce two luminance-aware modality adaptation strategies. These methods are particularly effective in scenarios where the RGB modality becomes unreliable (e.g. low-light). The full fusion strategy computes the mean luminance of the entire RGB image and adjusts the fusion weights globally based on this value. In contrast, the pixelwise fusion method computes luminance at each individual pixel, allowing for spatially adaptive blending that emphasizes the GAN-generated image in darker regions while preserving real RGB content in well-lit areas. Given an RGB input image  $\mathbf{I}_{\text{RGB}} \in \mathbb{R}^{H \times W \times 3}$ , The pixel values are normalized to the range  $[0, 1]$  and converted to grayscale using the Rec. 709 luminance formula:

$$\mathbf{I}_{\text{gray}}(u, v) = 0.2126 \cdot R(u, v) + 0.7152 \cdot G(u, v) + 0.0722 \cdot B(u, v) \quad (6)$$

For the full fusion we compute the mean luminance of the grayscale image to determine scene brightness:

$$L_{\text{mean}} = \frac{1}{HW} \sum_{u=1}^W \sum_{v=1}^H \mathbf{I}_{\text{gray}}(u, v) \quad (7)$$

Two threshold values,  $L_{\text{low}}$  and  $L_{\text{high}}$ , define a luminance band that guides modality fusion. Specifically:

- If  $L_{\text{mean}} \leq L_{\text{low}}$ , the RGB input is considered too dark and the GAN image is used.
- If  $L_{\text{mean}} \geq L_{\text{high}}$ , the RGB image is considered reliable and used directly.
- If  $L_{\text{mean}} \in (L_{\text{low}}, L_{\text{high}})$ , we compute a weighted linear blend between the two:

$$\alpha = \frac{L_{\text{mean}} - L_{\text{low}}}{L_{\text{high}} - L_{\text{low}}} \quad (8)$$

$$\mathbf{I}_{\text{fused}} = \alpha \cdot \mathbf{I}_{\text{RGB}} + (1 - \alpha) \cdot \mathbf{I}_{\text{GAN}} \quad (9)$$

As an alternative, we can apply pixel-wise blending by computing  $\alpha(u, v)$  for each pixel individually based on its local luminance:

$$\alpha(u, v) = \text{clamp}\left(\frac{\mathbf{I}_{\text{gray}}(u, v) - L_{\text{low}}}{L_{\text{high}} - L_{\text{low}}}, 0, 1\right) \quad (10)$$

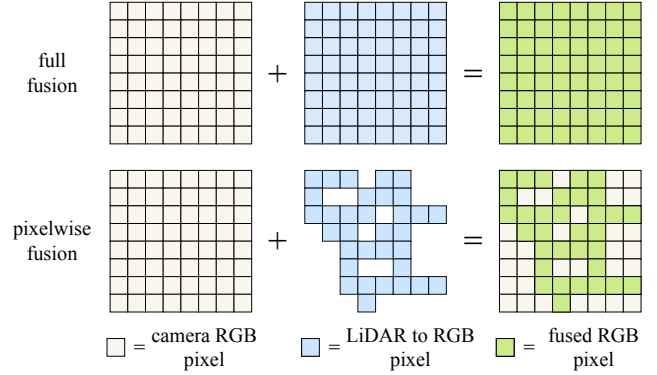


Fig. 3: Overview of the two modality fusion strategies used for combining RGB and LiDAR inputs. **(a) full fusion** applies a single global weighting factor to the entire RGB and LiDAR images, determined by the mean luminance of the RGB input. **(b) pixelwise fusion** computes a spatially varying weight map based on per-pixel luminance, allowing the model to blend information locally and adaptively. This enables fine-grained emphasis on LiDAR in poorly lit regions while still leveraging RGB information in well-exposed areas.

Here,  $\text{clamp}(x, 0, 1)$  restricts the value of  $x$  to the range  $[0, 1]$ , ensuring valid blending weights. This allows for spatially adaptive fusion, where dark regions rely more on the GAN image, while well-lit areas retain real RGB content.

This approach enables spatially adaptive fusion, where darker regions are blended more heavily with the GAN-generated image, while well-lit areas retain the original RGB content. In practice, we set the luminance thresholds to  $L_{\text{low}} = 0.15$  and  $L_{\text{high}} = 0.35$ , allowing for a smooth and continuous transition between modalities under varying illumination conditions. Figure 3 illustrates the two main fusion strategies: full-image (global) fusion and pixelwise (local) blending. By leveraging luminance cues, the system adaptively reduces reliance on unreliable RGB input in challenging scenarios—such as nighttime scenes, tunnels, or occluded environments—thereby enabling robust, context-aware multimodal perception.

#### D. VLM Integration

The final stage of the DepthVision pipeline fuses multimodal sensor data into a unified VLM, enabling high-level scene understanding across diverse environments.

*Inputs.*: The system takes the following inputs:

- **LiDAR point cloud:** A set of 3D points  $\mathbf{P} = \{\mathbf{p}_i\} \subset \mathbb{R}^3$ , which are later projected into a single-channel tensor  $\mathbf{I}_{\text{LiDAR}} \in \mathbb{R}^{1 \times H \times W}$ .
- **RGB image:** A 3-channel tensor  $\mathbf{I}_{\text{RGB}} \in \mathbb{R}^{3 \times H \times W}$  captured directly from the camera, resized to  $H = W = 600$  and normalized to  $[0, 1]$ .
- **Text input:** A sequence of token embeddings  $\mathbf{T} = \{\mathbf{t}_1, \dots, \mathbf{t}_n\} \subset \mathbb{R}^d$ , where  $n$  is the number of language tokens and  $d$  is the embedding dimension.

*Modality Adaptation.*: Based on LAMA, as described in Section III-C, we dynamically adapt the visual input to the VLM depending on the reliability of the RGB sensor. If the RGB image is well-exposed, it is passed directly to the model. In low-visibility conditions, we substitute the RGB view with a synthetic image generated by the LiDAR-to-RGB GAN. In intermediate cases, we blend the two sources using a luminance-dependent mixing coefficient. The resulting image  $\mathbf{I}_{\text{fused}}$  is converted back to standard RGB format and is suitable for direct processing by frozen VLMs.

*Transformer Input.*: The final image  $\mathbf{I}_{\text{fused}}$  is tokenized using a standard patch embedding module (e.g., from a Vision Transformer) to produce a sequence of  $N = \frac{H \cdot W}{P^2}$  image tokens, where  $P$  is the patch size. These visual tokens are concatenated with the embedded language tokens:

$$\mathbf{Z} = \text{Transformer}([\text{PatchEmbed}(\mathbf{I}_{\text{fused}}); \mathbf{T}]) \quad (11)$$

Importantly, the luminance-based adaptation operates entirely outside the VLM, requiring no fine-tuning and maintaining full compatibility with frozen vision–language backbones.

*Robustness Through Redundancy.*: By allowing the system to switch its emphasis between RGB and LiDAR based on observed luminance, DepthVision achieves robustness in adverse visual conditions such as:

- Poor lighting (e.g., nighttime or tunnels)
- Visual artifacts (e.g., glare, shadows, overexposure)
- Sensor dropout

*Output.*: The VLM produces task-specific outputs such as scene captions, object classes, or navigation decisions. This design makes DepthVision adaptable for a wide range of downstream applications in robotics, autonomous driving and perception in general.

## IV. EXPERIMENTS

We conduct experiments to evaluate the performance of DepthVision, both in terms of the bare image from depth generation and in terms of the full pipeline, including VLM scene understanding. For this purpose, we use real and synthetic data.

#### A. Implementation Details

To ensure reproducibility, we provide detailed descriptions of the model architectures and training configurations used in our experiments. The LiDAR-to-RGB synthesis pipeline is based on the conditional GAN framework introduced in pix2pix [29]. We have extended this framework by adding an extra convolutional layer and integrating a lightweight residual refiner module which enhances the quality and structural consistency of the generated images. All input images are resized to  $512 \times 512$  pixels and normalized to the range  $[-1, 1]$ . Training is conducted using mixed-precision arithmetic on NVIDIA GPUs to improve performance and memory efficiency.

For multimodal scene understanding, we evaluate state-of-the-art Vision–Language Models VLMs without fine-tuning. Specifically, we include *LLaVA-1.6-Mistral-7B* [32] and *Qwen2-VL-7B-Instruct* [33], both of which offer strong performance on open-ended visual reasoning and instruction-following tasks. Additionally, we wrap the Vision–Language Models in an architecture inspired by the *EMMA* architecture [34], implemented using the official *OpenEMMA* codebase [35].

#### B. Datasets and Training Details

*Sensor Setup.*: We train two separate DepthVision networks: one using simulation-based data from CARLA [36] and another using real-world data from the nuScenes dataset [37]. Table I outlines the key sensor specifications for both configurations.

TABLE I: Sensor specifications for simulation and real-world datasets.

Parameter	CARLA	nuScenes
Camera - Position	x: 1.8 m, z: 1.7 m*	Roof front
Camera - Resolution	800×600 px	1600×900 px
Camera - Field of View	90° horiz.	~70° horiz.
Camera - Frame Rate	5 Hz	12 Hz
LiDAR - Position	x: 1.8 m, z: 1.7 m*	Roof center
LiDAR - Channels	64	32
LiDAR - FOV	90° horiz., 74° vert.	360° horiz., 40° vert.
LiDAR - Range	100 m	70–120 m
LiDAR - Frame Rate	10 Hz	20 Hz
LiDAR - Points / Second	256k	~300k
Training - Samples	5744	28130

\*Positions are relative to the vehicle center.

To ensure consistent lighting conditions during training, we filter out samples with a mean luminance below 0.4. This ensures that the LiDAR-to-RGB synthesis network learns to generate primarily day-like images, thereby avoiding overfitting to poorly illuminated or low-information scenes. While the CARLA environment features a simplified test map with reduced complexity, the nuScenes-based model is trained and evaluated on more diverse and challenging real-world scenarios. The front camera and LiDAR are calibrated using known extrinsic and intrinsic parameters. For nuScenes, we densify the sparse point cloud by fusing up to three sequential LiDAR sweeps using vehicle odometry before projection.



*Training and Hyperparameters:* All components of the LiDAR-to-RGB synthesis pipeline—the generator, discriminator and refiner—are trained jointly using a combination of adversarial and reconstruction objectives. The total loss consists of a binary cross-entropy adversarial term and an  $L_1$  reconstruction loss scaled by a factor of 100, encouraging both structural accuracy and color fidelity.

Training is performed using the Adam optimizer [38] with  $\beta_1 = 0.5$ ,  $\beta_2 = 0.999$  and a learning rate of  $2 \times 10^{-4}$ . A batch size of 16 is used and mixed-precision arithmetic is employed to improve computational efficiency and memory usage. The training process is parallelized across two NVIDIA RTX 4090 GPUs. The full set of training hyperparameters is summarized in Table II.

TABLE II: Training hyperparameters.

Parameter	Value
Optimizer	Adam ( $\beta_1 = 0.5$ , $\beta_2 = 0.999$ )
Learning rate	$2 \times 10^{-4}$
Batch size	16
Epochs	200
Loss functions	Adversarial + $L_1$
$L_1$ loss weight ( $\lambda$ )	100
Input scaling	RGB pixel values normalized to $[-1, 1]$
Luminance threshold	0.4 (low-light filter)

### C. Simulation

In order to evaluate LiDAR-to-RGB synthesis in low-light settings, we designed a dedicated night-time evaluation environment in CARLA. Scenes were generated using fixed geometry, calibrated sensors and minimal ambient illumination to mimic real-world visibility degradation, while ensuring precise alignment between the LiDAR and RGB modalities. Notably, the DepthVision model was trained exclusively on daytime data, enabling it to generate daytime-like images in previously unseen night-time conditions.

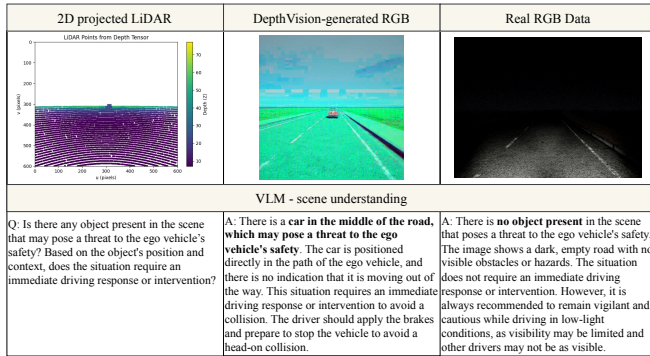


Fig. 4: Simulation evaluation. A nighttime highway scenario shows a vehicle ahead at a safety-critical distance requiring braking. Due to inactive lights, the vehicle is not visible in the real image. In contrast, the DepthVision-generated image clearly reveals the vehicle, enabling the VLM (QWEN) to reason correctly and suggest braking.

LiDAR scans from the night-time environment were processed through the DepthVision pipeline to generate synthetic RGB images. As shown in Fig. 4, the model successfully preserves critical semantic and structural cues,

such as lane markings, vehicle contours and scene layout, despite the sparsity of the input. The generator produces plausible textures and colors based on depth geometry, while the refiner improves edge sharpness and reduces artifacts. In many cases, synthetic images provide better visibility than raw night-time RGB captures, as they compensate for sensor noise and glare using information learned from well-lit scenes. This structure provides a robust visual signal for reasoning in adverse conditions.

### D. Baseline

To enable a controlled comparison with our proposed DepthVision framework, we construct a baseline system focused on front-view multimodal scene understanding using large-scale VLMs. This baseline is modeled after NuScenes-QA [39], but is adapted to single-frame, real-world settings with calibrated LiDAR and RGB inputs.

*Dataset Composition.:* We curated a subset of 100 samples from the nuScenes validation set [37], selecting 50 day and 50 night scenes from the front camera perspective. Each sample includes a single RGB image, the corresponding LiDAR sweep and complete calibration metadata. The LiDAR sweep was cropped to fit the camera's field of view.

*Question Types and Annotation.:* Each image is paired with manually authored question-answer (QA) pairs, that can be categorized in three classes as:

- **Existence (Safety Critical):** Questions that ask for the number of safety-critical objects in the scene (e.g., vehicles in close proximity that may pose a collision risk), requiring accurate object detection and counting.
- **Count:** Questions that require counting the number of objects in a specific class (e.g., cars, trucks, pedestrians or motorcycles).
- **Object Classification:** Questions that ask for the classification of an object, often based on its spatial relation to other objects or scene context.
- **Acc:** The overall Top-1 accuracy, computed as the average across all three tasks above.

Ground truth labels are derived from a combination of human annotations and nuScenes 3D bounding boxes, cross-validated via projected sensor views for spatial consistency. All models are evaluated in zero-shot mode without fine-tuning, using GAN-generated images and corresponding natural language queries. Evaluation metrics include Top-1 accuracy across QA categories. This setup provides a reproducible benchmark for understanding scenes across multiple modalities and facilitates the quantitative evaluation of the impact of DepthVision.

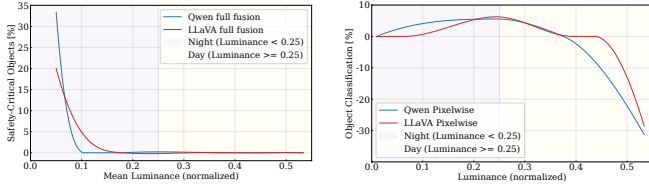
### E. Real-World Performance

We evaluate the effectiveness of our LiDAR-augmented visual reasoning framework on real world data by comparing baseline Vision-Language Model VLM performance under three visual input conditions: (i) camera-only (RGB) and two versions of DepthVision (ii) RGB + LiDAR via full fusion and (iii) RGB + LiDAR via pixelwise fusion. Table III shows the quantitative results for three reasoning tasks — existence

TABLE III: Top-1 accuracy of vision–language models using camera and LiDAR-to-RGB synthesis under varying fusion strategies and lighting conditions.

VLM	DataSource (fusion strategy)	Exist (Safety Critical)			Count			Object			Acc		
		Day	Night	All	Day	Night	All	Day	Night	All	Day	Night	All
QWEN	Camera-only	54.8	53.3	54.1	86.9	88.3	87.6	94.7	74.7	84.7	78.8	72.1	75.5
QWEN	Camera + LiDAR (full)	54.8 <sup>†</sup>	<b>66.7</b>	<b>60.8</b>	86.9 <sup>†</sup>	84.5	85.7	94.7 <sup>†</sup>	73.1	83.9	78.8 <sup>†</sup>	74.8	<b>76.8</b>
QWEN	Camera + LiDAR (pixelwise)	47.6	44.4	46.0	77.4	85.5	81.5	63.2	<b>80.7</b>	72.0	62.7	70.2	66.5
LLAVA	Camera-only	83.0	57.8	70.4	79.9	78.3	79.1	68.4	57.7	63.1	77.1	64.6	70.9
LLAVA	Camera + LiDAR (full)	83.0 <sup>†</sup>	<b>73.3</b>	<b>78.2</b>	79.9 <sup>†</sup>	<b>83.9</b>	81.9	68.4 <sup>†</sup>	53.8	61.1	77.1 <sup>†</sup>	70.3	<b>73.7</b>
LLAVA	Camera + LiDAR (pixelwise)	82.9	60.0	71.5	85.4	79.4	82.4	55.0	<b>61.6</b>	58.3	74.4	67.0	70.7

<sup>†</sup>Same as Camera-only. Fusion was not applied during daytime scenes when using full fusion.



(a) Relative accuracy improvement in detecting safety-critical objects when using DepthVision with full weighted fusion compared to camera-only input.

(b) Relative improvement in object classification accuracy with pixelwise weighted fusion compared to camera-only.

Fig. 5: Performance gains as a function of scene luminance: comparison between RGB-only and DepthVision-enhanced inputs for (a) safety-critical detection and (b) general object classification tasks.

(safety-critical), object counting and object classification — under both day and night conditions.

*LiDAR Augmentation Improves Low-Light Scene Understanding.*: As shown in Table III, augmenting RGB inputs with LiDAR-generated imagery significantly enhances VLM performance under low-luminance conditions. In particular, fusing the refiner GAN-generated LiDAR image via full fusion substantially improves the accuracy of safety-critical object detection at night for Qwen2-VL-7B-Instruct (from 53.3% to 66.7%, a **13.4%** absolute improvement) and for LLaVA-1.6-Mistral-7B, an improvement of **15.5%**. This pattern is consistent across models, indicating that the additional structural information from LiDAR mitigates the degradation in RGB image quality at night.

*Fusion Strategy Matters: Full vs. Pixelwise Fusion.*: The experimental results indicate that, in general, full fusion outperforms pixel-wise fusion across most tasks. Notably, pixel-wise fusion yields a relative improvement of up to **6 %** in object classification, suggesting its effectiveness in preserving fine-grained object details under low-light conditions by locally enhancing dark regions. However, this localized blending can introduce inconsistencies in well-lit scenes, occasionally degrading performance during daytime scenarios. In contrast, full fusion provides a more stable and globally consistent representation across varying lighting conditions

*Luminance-Aware Performance Trends.*: To better understand the effect of ambient lighting on model performance,

we compute the mean luminance of each input image and analyze its correlation with VLM accuracy. Figure 5 shows separate performance trends for each task (Safety Critical and Object Classification), comparing RGB-only inputs with fused RGB+LiDAR inputs. The results reveal several key patterns:

- A consistent improvement in performance under low-light (nighttime) conditions when using fused inputs.
- A performance drop during the daytime when using pixel-wise fusion, which is likely due to suboptimal blending in uniformly well-lit scenes. This may be because frozen VLMs are not trained to process such fused inputs, which leads to distribution shifts. Disabling fusion above a defined luminance threshold can mitigate this issue.
- Increasing performance differences between RGB-only and fused inputs as luminance decreases, highlighting the complementary role of LiDAR in poor visibility scenarios.

*Task-Specific Gains.*: The most significant impact of LiDAR augmentation is seen in safety-critical detection tasks, where structural cues, such as object boundaries and contours, are vital for identifying obscured or dimly lit vehicles and pedestrians. The Count and Object Classification tasks also demonstrate greater robustness, particularly in challenging night-time conditions. These results reinforce the central hypothesis of this work: that real-time LiDAR-guided RGB synthesis can enhance downstream multimodal reasoning in low-visibility scenarios, without requiring retraining or architectural modifications to existing Vision–Language Models.

## V. LIMITATIONS

While DepthVision enhances robustness in low-light conditions, certain visual cues remain challenging to capture or interpret through synthesized imagery alone. Color information remains essential in specific scenarios, such as reading traffic signs with similar shapes but different text or colors (e.g., speed limits). Additionally, fine-grained visual cues such as eye gaze, facial expressions and subtle body movements play a critical role in interpreting human intent during human–machine interaction.

## VI. CONCLUSION

We presented DepthVision, a robust, multimodal framework that facilitates reliable vision-language reasoning for robotics in challenging sensing conditions. At its core, the system employs a GAN-based LiDAR-to-RGB synthesis network with an integrated refiner to produce realistic images from sparse depth data. These synthetic views are then combined with real camera input via a Luminance-Aware Modality Adaptation (LAMA) that adaptively fuses the two types of input based on scene brightness. This approach improves perception in scenarios where RGB input is degraded, such as at night or in low-luminance environments, while remaining fully compatible with frozen Vision-Language Models. Experimental results confirm that our method significantly improves performance in safety-critical and object-level robotic tasks, particularly at night, without the need for VLM retraining.

## REFERENCES

- [1] H. Jeong, J. Shin, F. Rameau, and D. Kum, "Multi-modal place recognition via vectorized hd maps and images fusion for autonomous driving," *IEEE Robotics and Automation Letters*, vol. 9, no. 5, pp. 4710–4717, 2024.
- [2] A. R. Sekkat, R. Mohan, O. Sawade, E. Matthes, and A. Valada, "Amodalsynthdrive: A synthetic amodal perception dataset for autonomous driving," *IEEE Robotics and Automation Letters*, 2024.
- [3] D. Zhang *et al.*, "Pep: Policy-embedded trajectory planning for autonomous driving," *IEEE Robotics and Automation Letters*, 2024.
- [4] S. Mozaffari, M. A. Sormoli, K. Koufos, and M. Dianati, "Multimodal manoeuvre and trajectory prediction for automated driving on highways using transformer networks," *IEEE Robotics and Automation Letters*, vol. 8, no. 10, pp. 6123–6130, 2023.
- [5] S. Kim, H. Jeon, J. W. Choi, and D. Kum, "Diverse multiple trajectory prediction using a two-stage prediction network trained with lane loss," *IEEE Robotics and Automation Letters*, vol. 8, no. 4, pp. 2038–2045, 2022.
- [6] R. Greer, N. Deo, and M. Trivedi, "Trajectory prediction in autonomous driving with a lane heading auxiliary loss," *IEEE Robotics and Automation Letters*, vol. 6, no. 3, pp. 4907–4914, 2021.
- [7] D. Driess *et al.*, "Palm-e: an embodied multimodal language model," in *Proceedings of the 40th International Conference on Machine Learning*, ser. ICMML'23. JMLR.org, 2023.
- [8] A. Vaswani *et al.*, "Attention is all you need," *Advances in neural information processing systems*, vol. 30, 2017.
- [9] A. Brohan *et al.*, "Rt-1: Robotics transformer for real-world control at scale," in *arXiv preprint 2212.06817*, 2022.
- [10] Y. Jiang *et al.*, "VIMA: Robot manipulation with multimodal prompts," in *Proceedings of the 40th International Conference on Machine Learning*, ser. Proceedings of Machine Learning Research, vol. 202. PMLR, 23–29 Jul 2023, pp. 14 975–15 022.
- [11] X. Zhai, A. Kolesnikov, N. Houlsby, and L. Beyer, "Scaling vision transformers," in *Proceedings of the IEEE/CVF conference on computer vision and pattern recognition*, 2022, pp. 12 104–12 113.
- [12] Alayrac *et al.*, "Flamingo: a visual language model for few-shot learning," *Advances in neural information processing systems*, vol. 35, pp. 23 716–23 736, 2022.
- [13] B. Chen *et al.*, "Spatialvlm: Endowing vision-language models with spatial reasoning capabilities," in *Proceedings of the IEEE/CVF Conference on Computer Vision and Pattern Recognition*, 2024, pp. 14 455–14 465.
- [14] T. Kwon, N. Di Palo, and E. Johns, "Language models as zero-shot trajectory generators," *IEEE Robotics and Automation Letters*, vol. 9, no. 7, pp. 6728–6735, 2024.
- [15] N. Wake, A. Kanehira, K. Sasabuchi, J. Takamatsu, and K. Ikeuchi, "Gpt-4v (ision) for robotics: Multimodal task planning from human demonstration," *IEEE Robotics and Automation Letters*, 2024.
- [16] A. Mei, G.-N. Zhu, H. Zhang, and Z. Gan, "Replanvlm: Replanning robotic tasks with visual language models," *IEEE Robotics and Automation Letters*, 2024.
- [17] D. Song *et al.*, "Vlm-social-nav: Socially aware robot navigation through scoring using vision-language models," *IEEE Robotics and Automation Letters*, 2024.
- [18] J. Wen *et al.*, "Tinyvla: Towards fast, data-efficient vision-language-action models for robotic manipulation," *IEEE Robotics and Automation Letters*, 2025.
- [19] M. R. Loghmani, M. Planamente, B. Caputo, and M. Vincze, "Recurrent convolutional fusion for rgb-d object recognition," *IEEE Robotics and Automation Letters*, vol. 4, no. 3, pp. 2878–2885, 2019.
- [20] A. Dosovitskiy *et al.*, "An image is worth 16x16 words: Transformers for image recognition at scale," in *9th International Conference on Learning Representations, ICLR 2021*, 2021.
- [21] A. Radford *et al.*, "Learning transferable visual models from natural language supervision," in *International conference on machine learning*. Pmlr, 2021, pp. 8748–8763.
- [22] L. H. Li, M. Yatskar, D. Yin, C.-J. Hsieh, and K.-W. Chang, "Visualbert: A simple and performant baseline for vision and language," *arXiv preprint arXiv:1908.03557*, 2019.
- [23] A. Singh, R. Hu, V. Goswami, G. Couairon, W. Galuba, M. Rohrbach, and D. Kiela, "Flava: A foundational language and vision alignment model," in *Proceedings of the IEEE/CVF conference on computer vision and pattern recognition*, 2022, pp. 15 638–15 650.
- [24] L. Chen *et al.*, "Driving with llms: Fusing object-level vector modality for explainable autonomous driving," in *2024 IEEE International Conference on Robotics and Automation (ICRA)*, 2024, pp. 14 093–14 100.
- [25] S. Yang *et al.*, "Lidar-llm: Exploring the potential of large language models for 3d lidar understanding," in *Proceedings of the AAAI Conference on Artificial Intelligence*, vol. 39, no. 9, 2025, pp. 9247–9255.
- [26] I. J. Goodfellow *et al.*, "Generative adversarial nets," *Advances in neural information processing systems*, vol. 27, 2014.
- [27] A. Radford, L. Metz, and S. Chintala, "Unsupervised representation learning with deep convolutional generative adversarial networks," *arXiv preprint arXiv:1511.06434*, 2015.
- [28] O. Ronneberger, P. Fischer, and T. Brox, "U-net: Convolutional networks for biomedical image segmentation," in *International Conference on Medical image computing and computer-assisted intervention*. Springer, 2015, pp. 234–241.
- [29] P. Isola, J.-Y. Zhu, T. Zhou, and A. A. Efros, "Image-to-image translation with conditional adversarial networks," in *Proceedings of the IEEE conference on computer vision and pattern recognition*, 2017, pp. 1125–1134.
- [30] A. Shrivastava, T. Pfister, O. Tuzel, J. Susskind, W. Wang, and R. Webb, "Learning from simulated and unsupervised images through adversarial training," in *Proceedings of the IEEE conference on computer vision and pattern recognition*, 2017, pp. 2107–2116.
- [31] J. Adler and O. Öktem, "Solving ill-posed inverse problems using iterative deep neural networks," *Inverse Problems*, vol. 33, no. 12, p. 124007, 2017.
- [32] F. Li *et al.*, "Llava-next: Tackling multi-image, video, and 3d in large multimodal models," <https://llava-vl.github.io/blog/2024-06-16-llava-next-interleave/>, June 2024, accessed: Aug. 2, 2025.
- [33] P. Wang *et al.*, "Qwen2-vl: Enhancing vision-language model's perception of the world at any resolution," *arXiv preprint arXiv:2409.12191*, 2024.
- [34] J.-J. Hwang *et al.*, "Emma: End-to-end multimodal model for autonomous driving," *arXiv preprint arXiv:2410.23262*, 2024.
- [35] S. Xing *et al.*, "Openemma: Open-source multimodal model for end-to-end autonomous driving," in *Proceedings of the Winter Conference on Applications of Computer Vision*, 2025, pp. 1001–1009.
- [36] A. Dosovitskiy, G. Ros, F. Codevilla, A. Lopez, and V. Koltun, "Carla: An open urban driving simulator," in *Conference on robot learning*. PMLR, 2017, pp. 1–16.
- [37] H. Caesar *et al.*, "nuscenes: A multimodal dataset for autonomous driving," in *Proceedings of the IEEE/CVF conference on computer vision and pattern recognition*, 2020, pp. 11 621–11 631.
- [38] D. P. Kingma and J. Ba, "Adam: A method for stochastic optimization," in *3rd International Conference on Learning Representations, ICLR 2015, San Diego, CA, USA, May 7-9, 2015*.
- [39] T. Qian, J. Chen, L. Zhuo, Y. Jiao, and Y.-G. Jiang, "Nuscenes-qa: A multi-modal visual question answering benchmark for autonomous driving scenario," in *Proceedings of the AAAI Conference on Artificial Intelligence*, vol. 38, no. 5, 2024, pp. 4542–4550.